

This discussion paper is/has been under review for the journal Atmospheric Chemistry and Physics (ACP). Please refer to the corresponding final paper in ACP if available.

Characterization of ions at Alpine waterfalls

P. Kolarž^{1,*}, M. Gaisberger^{2,*}, P. Madl³, W. Hofmann³, M. Ritter², and A. Hartl²

¹Institute of Physics, University of Belgrade, Pregrevica 118, 11080 Belgrade, Serbia

²Paracelsus Medical University, Institute for Physiology and Pathophysiology, Strubergasse 21, 5020 Salzburg, Austria

³University of Salzburg, Department of Materials Research and Physics, Division of Physics and Biophysics, Hellbrunner Str. 34, 5020 Salzburg, Austria

*These authors contributed equally to this work.

Received: 16 June 2011 – Accepted: 4 September 2011 – Published: 9 September 2011

Correspondence to: P. Kolarž (kolarz@ipb.ac.rs)

Published by Copernicus Publications on behalf of the European Geosciences Union.

25297

Abstract

During a three-year field campaign of measuring waterfall generated ions, we monitored five different waterfalls in the Austrian Alps. Most measurements were performed at the Krimml waterfall (Salzburg), which is the biggest and most visited one in Europe and the Gartl waterfall (Mölltal, Carinthia). Smallest ion sizes (0.9–2 nm) were measured with a cylindrical air ion detector (CDI-06) while ion sizes from 5.5 to 350 nm were measured using a modified Grimm SMPS aerosol spectrometer. Measurements showed high negative ion gradients nearby waterfalls whereas positive ions showed only a moderate increase. The most abundant sizes of nano-sized and sub-micrometer ions measured were at 2 nm and of the larger and heavier ones at 120 nm.

1 Introduction

1.1 Air ions in the environment

The term “air ions” refers to all charged airborne particles that have electrical mobility. In general, they are continually created by natural sources such as cosmic rays, radioactive decay of noble gases (such as radon) in the air and radioactive minerals from the ground. After the ionization process and in a very short time (typically microseconds) primary ions evolve via a process of hydration and ion cluster formation into complexes known as small air ions (charged nano-aerosols) with a lifetime of up to 100 s. The central ion of a cluster could contain one inorganic molecule and be surrounded by one layer of water molecules. However, due to the purity of the water, such inactivation cores are largely absent in the aerosols of the waterfalls (WF) investigated. The background concentration of air ions in the environment is about a few hundred per cubic centimetre with an average near-ground ionization rate of 10 ion pairs $\text{cm}^{-3} \text{s}^{-1}$.

25298

polarizing voltage (U) and air flow:

$$\mu_c = \frac{V_S (R_2^2 - R_1^2) \ln(R_2/R_1)}{2LU} \quad (2)$$

where R_2 and R_1 are the radii of the polarizing and collecting electrode; L is the collecting electrode length and V_S is the air velocity through the electrodes. Air-flow and polarizing voltage on 3 detectors were set to measure air ions in size ranges ≤ 0.9 , 1.5 and 2 nm (Eq. 2). These three values are depicted due to characteristic sizes of ions created by WF, which is around 2 nm (Laakso et al., 2007) and by nuclear decay as well as cosmic rays – with the latter up to 0.9 nm. It is expected that simultaneous measurements of all three instruments on places where no WF-related ions are present should show approximate air ion concentrations. The instrumental uncertainties under regular conditions are about 5 % (Kolarž et al., 2009). Taking into account the extreme and difficult conditions during the field campaign and particularly near the WFs, an additional uncertainty should be added. Yet, efforts, such as maintaining constant RPM of the fans, thermostated electronics and electrodes, use of additional protective case and manual zeroing procedure have been employed to limit uncertainties to additional 10 %. Altogether, by using the “root-sum-of-squares” method the overall uncertainty amounts to 11 %.

Air ion particles in the size range from 5.5 to 358 nm were measured with the Grimm SMPS (Scanning Mobility Particle Sizer) using an M-DMA (Medium-Differential Mobility Analyzer) for size class differentiation and an attached CPC (Condensation Particle Counter) to quantify the particle concentration. Within the DMA, the particles are selected according to their electrical mobility, which is accomplished using a ^{241}Am radioactive source mounted on the DMA air inlet. To avoid neutralization of the aerosolised ions, this so-called “neutralizer” was detached from the M-DMA. Doing so one obtains an SMPS detector that is able to count negatively charged particles. The entire system was operated with a backup battery power supply enabling 8 h of uninterrupted operation in the field.

25301

Atmospheric data like temperature and wind speed were measured by a PCE-007 anemometer attached to a data logger.

Measurement of ion concentrations in the vicinity of the WF is difficult and restricted due to the existence of dispersed drops in the air (water aerosols). These droplets are not only contributing to the increase in relative humidity but also in wetting the instruments, soaking the electrodes of the CDI, thereby causing current leakages in the electrode system and amplifying electronics.

In addition, the temperature gradient at the falls results in a heavy surge, which is directed away from the WF downstream in periodical gusts – especially at the Krimml WF. These gusts are carrying water aerosols, and are usually, but not always, higher loaded with air ions. Periods of intense gusts are followed by modest ones and typically last for a few tens of seconds.

These conditions limit the duration of the measurements and act as a delimiting factor when attempting to obtain a comprehensive outline of the inventory at the falls. All these difficulties were partially avoided by encasing the CDI instruments in aluminium boxes with inlets for the probes and outlet for exhaust and excess heat. These cases also contributed to the protection of control- and supply units. The SMPS was also operated in a sealed housing, thus only the inlet was subject to excessive humidity. All instruments were mounted onto a 4-wheel trolley fitted with a tow rail (Fig. 2). It is small enough to be loaded onto a pick-up truck in order to approach different falls at different off-road locations.

3 Measurements and discussion

3.1 Study of 5 different WFs

During the summer of 2008, five WFs in Austria were studied and compared with control sites where WF-related ions were not present. Table 1 shows average and maximal number concentrations of positive and negative air ions of 4 alpine and one artificial

25302

WF. All WF ion concentrations were measured at places of maximal ionization and moderate wetting of the instruments. The highest average concentration increase of 2 nm-sized negative ions – in comparison to control point's concentration – was found to be 80-fold.

5 WF ion concentrations fluctuate depending on measuring sites, but their averages at the examined sites typically depend on the quantity of water flow, which varies seasonally. In contrast, the origin and structure of the ions generated at reference sites arise mostly from natural radioactivity, which is subject to diurnal changes (Kolarž et al., 2009; Chandrashekara, et al., 2006). Accordingly, the presented relations between
10 WF and background ions vary diurnally and seasonally.

The data in Table 1 lead to the conclusion that the production of WF ions not only depends on the height of the WF and its quantity of water flowing per unit of time, but also on the location of the WF, the surrounding topography, and of course, the location of the measuring points.

15 Larger WFs create periodical gusts, which are usually carrying a lot of water droplets that can be seen with the naked eye and likewise felt on the skin. These gusts do not necessarily carry small water droplets but when they do, the resulting increase in concentration of WF-generated ions are immediately detected by the instruments. This is especially significant at the Krimml WF where three falling cascades generate very
20 complex air-flow patterns.

Figure 3 shows the artificial WF with a cascade that is 5 m high on the river Möll. Although ion concentrations are 11-fold higher than background measurements, they are much lower than any of the higher WFs (Table 1). This supports the assumption that one of the processes that contribute to WF ion generation is charge separation
25 via aerodynamic break-up of micrometer-sized water droplets into nano-sized aerosols (Zilch et al., 2008). Another mechanism regards the rapid decline in relative humidity as the aerosolised droplets drift further off the WF. This implies that if the particle size is larger than the Kelvin diameter, the aerosol particles will grow; if the particle size is smaller, they will evaporate.

25303

Hence, as one moves away from the waterfall and due to the change in super-saturated conditions, the corresponding Kelvin droplet diameter becomes larger as under-saturated conditions are reached (decrease in relative humidity and increase
5 in temperature), which causes the aerosols to shrink in size, further accounting to a smaller particle sized diameter. However, the most prominent mechanism of formation is encountered when the water droplets hit a surface (water, or rock), thereby fragment and in combination with the above (bubble bursting effect, as shown in Fig. 1) yield
nano-sized aerosols.

3.2 Ion inventory at the Krimml WF

10 The Krimml WF is located in the northern region of the “Hohe Tauern” – a part of the eastern alpine region. It belongs to a glacial creek named “Krimmler Ache” whose water flows according to the season. In July the average throughput is about $20\,000\text{ m}^3\text{ h}^{-1}$, whereas it is only $500\text{ m}^3\text{ h}^{-1}$ in February. The WF itself consists of three consecutive cascades, with a height of 140 m, 100 m and 140 m high (Fig. 4). The base
15 of the WF is at an altitude of around 1100 m above sea level. The height of the last WF cascade provides maximal velocity to water droplets as the flow reaches 53 m s^{-1} . The chemical composition of the water reveals an almost neutral pH (7.36) with very low concentrations of Ca^{2+} (3.45 mg L^{-1}), Mg^{2+} (1.22 mg L^{-1}) and Cl^{-} (0.26 mg L^{-1}). The conductivity was $30\text{ }\mu\text{S cm}^{-1}$.

20 From a microbiological point of view, the water quality showed a moderate enraged count of colony forming units (100 CFU ml^{-1}). Simultaneous measurements of small clusters, intermediate and large ions created by the WF and natural ionizing radiation were performed – shown in Fig. 4 – over a two-week period in July 2010 on both sides of the bottom cascade at the Krimml WF.

25 To test the performance of the instrumentation, an inter-comparison between the cylindrical ion detectors was done (Fig. 5). Two detectors, with the same voltage and amplification settings, placed side by side, were used to measure negative ion concentration gradients near the Krimml WF. For that purpose, the trolley (Fig. 2) was used

25304

for translocation among the various sampling sites and for the slow approach to the nearest point of the orographic right side at the falls. The Figure reveals the Pearson correlation factor of $r = 0.97$, which is more than satisfactory considering the measuring conditions encountered during the campaign (Fig. 5). Testing was conducted also at different sites and locations.

Gradients of ≤ 2 nm size positive and negative air ion concentrations measured during the three-week field campaign at the Krimml WFs in July 2010 are shown in Fig. 6. Distances were measured from the base of the lowest cascade (using Google earth coordinates: 47.208283 N/12.170859 E). On the orographic right side, with the last measuring points being the reference site some 547 m away from the falls, assuming that no WF-related ions are present there. The reason for the relatively short gradient distance on the orographic left side is due to the dense forest cover that dominates the farther site some 228 m from the WF. The differences between the maximal values on the left and the right side of the WF, i.e. the creek, arise from the topographic configuration, the time variations when measurements were performed, turbulent air flows and varied solar flux within the upper Krimml valley.

All ion measurements were carried out at points that ensure that the instruments were not subject to instant flooding. Accordingly, the nearest measuring points were 57 m and 75 m on the orographic left and right side of the Krimml WF, respectively. Both measuring points are slightly shifted out of the main axis, which is directed sharply to the left orographic uphill side (Fig. 4 and aerial view of Fig. 6). The lower concentration on the left side is the result of complex turbulent air-flow generated by the huge amount of water pouring into the pond.

In comparison with the other WFs that we measured (Table 1), the maximal ion concentrations generated near the Krimml WF were apparently low, i.e. only about 20 times higher than the measured background, while maximal ion concentrations at the Gartl WF (Döllach) amounted to 6×10^4 ions cm^{-3} , i.e. 120 times higher than the measured background. Noteworthy for our field observation is that although the Krimml WF generates much more aerosols but fewer in the sub-nano-size range, wetting of

25305

the instrumentation is much more prevalent than at the other WFs. Due to the dynamics of waterfall generated aerosols, monitoring the inventory with a SMPS is not the first choice, as it requires a 120 s interval for the completion of a full scan. The ideal detector should at least measure in seconds intervals, like the ELPI. However this instrument – due to its weight and power requirements – makes field measurements a real challenge. In order to overcome this shortage, at least 3 full SMPS scans were made at every point, each divided into 44 size channels and each channel computed as an average of 9 individual recordings (out of which the 1st and the 9th are omitted as the system dynamically changes the voltage when switching from one size bin to the next). Using the SMPS and due to the nature of its detection principle it measures only negatively charged particles. Consequently, it deprived us from the ability to monitor the increase of positively charged aerosols in the 200 nm size range and beyond, as reported by Reiter (1994).

3.3 Ion measurements at the Krimml WF

Gradients of 0.9, 1.5 and 2 nm size positive and negative integral ion concentrations are shown in Fig. 7. As mentioned before, the non-linear decay function of the negative ion concentration is caused by the local topography and wind patterns. Positive ions did not reveal significant increases in concentrations and only 2 nm sized ions showed a nice correlation ($r = 0.6$) between positive and negative ions gradients. Interestingly enough, all three dimensions of positive ions were rising with distance within the first hundred meters from the waterfall only to decrease further afield. This is probably due to very high concentrations of negative ions as well as aerosols in the vicinity of the waterfall. This implies that higher coefficients of α and β (see Eq. 1) amplified by strong turbulent air flow patterns must be taken into consideration.

Equalization of the smallest positive and negative air ion concentrations is a signal that almost all WF-related negative ions are neutralized. The remaining ones can be traced back to the formation mechanisms usually associated to natural radioactivity and cosmic radiation. This is the case at the last point ($l = 547$ m) downstream from the WF

25306

- sition of waterfall-induced air ions, spectrometry vs. simulations, *Boreal. Environ. Res.*, 12, 409–420, 2007.
- Reiter, R.: Charges on particles of different size from bubbles of Mediterranean Sea surf and from waterfalls, *J. Geophys. Res.*, 99(D5), 10807–10812, 1994.
- 5 Takahashi, K., Otsuki, T., Mase, A., Kawado, T., Kotani, M., Ami, K., Matsushima, H., Nishimura, Y., Miura, Y., Murakami, S., Maeda, M., Hayashi, H., Kumagai, N., Shirahama, T., Yoshimatsu, M., and Morimoto, K.: Negatively-charged air conditions and responses of the human psycho-neuro-endocrino-immune network, *Environ. Int.*, 34(6), 765–772, 2008.
- 10 Tammet, H.: Size and mobility of atmospheric particles, clusters and ions, *J. Aerosol. Sci.*, 26, 459–475, 1995.
- Yamada, R., Yanoma, S., Akaike, M., Tsuburaya, A., Sugimasa, Y., Takemiya, S., Motohashi, H., Rino, Y., Takanashi, Y., and Imada, T.: Water-generated negative air ions activate NK cell and inhibit carcinogenesis in mice, *Cancer Lett.*, 239, 190–197, 2005.
- 15 Vostrikov, A. A., Drozdov, S. V., Rudnev, V. S., and Kurkina, L. I.: Molecular dynamics study of neutral and charged water clusters, *Comput. Mater. Sci.*, 35, 254–260, 2006.
- Zilch, L., Maze, J., Smith, J., Ewing, G., and Jarrold, M.: Charge separation in the aerodynamic breakup of micrometer-sized water droplets, *J. Phys. Chem. A.*, 112, 13352–13363, 2008.

25311

Table 1. Overview of the ion (≤ 2 nm) concentrations measured at closest range of the WFs and at control places (CP).

WF name	Average WF ion conc.		Max. WF ion conc.		Average ion conc. at ref. site		Conc. increase n_{WF}^-/n_{CP}^-	Conc. increase n_{WF}^+/n_{CP}^+
	[ions m ⁻³]		[ions m ⁻³]		[ions m ⁻³]			
	negative	positive	negative	positive	negative	positive		
Krimml	16581	1040	27540	1736	460	390	36	3
Stuiben	43913	2142	54359	3098	546	620	80	3
Bad Gastein	24748	1290	31606	428	774	510	32	3
Gartl	42660	1798	57510	2400	840	760	51	2
Artificial	3294	1446	6251	1582	306	544	11	3

25312

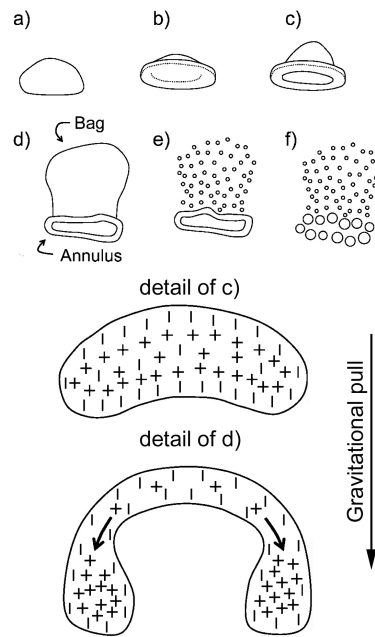


Fig. 1. Theoretical concept of the charge separation mechanism of a falling water droplet. Water bag formation (a–d), fracture into micro-bubbles (e–f) (modified according to Zilch et al., 2008).

25313



Fig. 2. Air ion detectors (left), SMPS, anemometer and GPS (middle) and field strength meter.

25314



Fig. 3. Artificial WF at the river Möll.

25315



Fig. 4. The last of three cascades at the Krimml WF.

25316

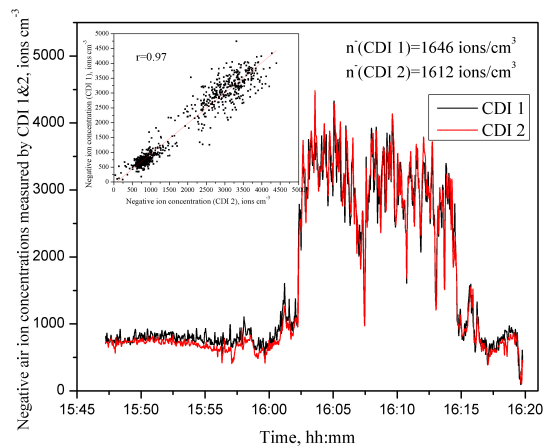


Fig. 5. Intercomparison of ion detectors (CDI-06) nearby Krimml WF versus time. Correlation factor 0.97.

25317

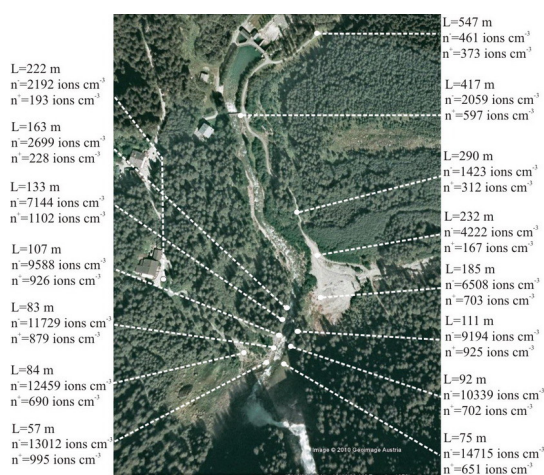


Fig. 6. Three-year summer average of 2 nm ion concentration gradients on both sides of the Krimml WF. The distances from the WF were measured via GPS and visualized on a Google Earth map.

25318

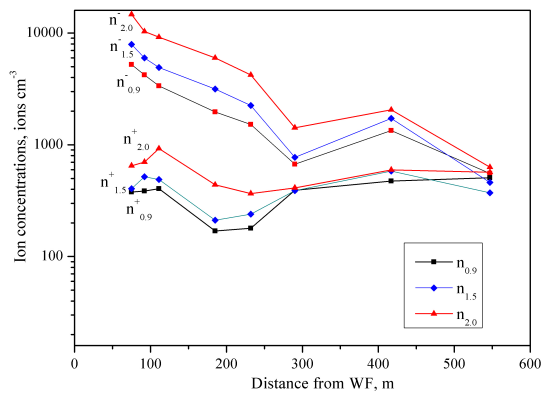


Fig. 7. Integral ion concentrations gradients by ion diameter and polarity measured on the orographic right side of the Krimml WF versus distance.

25319

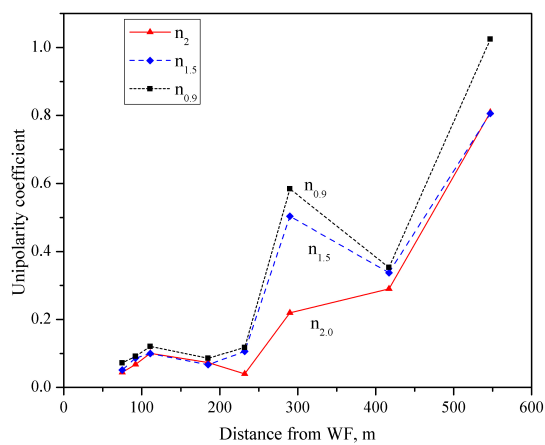


Fig. 8. Unipolarity coefficients for 3 different ion sizes versus distance measured at the Krimml WF.

25320

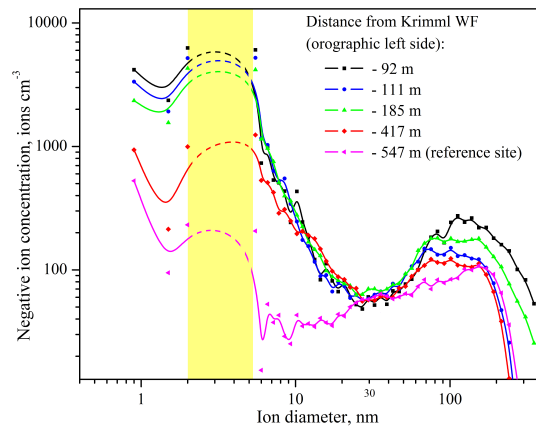


Fig. 9. Air ion concentrations vs. size for different distance measuring points at Krimml WF. Shaded area indicates interpolated values (cubic B-spline) between CDI-06 (0.9–2.0 nm) and SMPS (5.5–350 nm) measurements. The 547 m data series (magenta curve) represents the reference site where no WF generated ions were expected to occur.

25321



Fig. 10. Gartl WF with surroundings.

25322

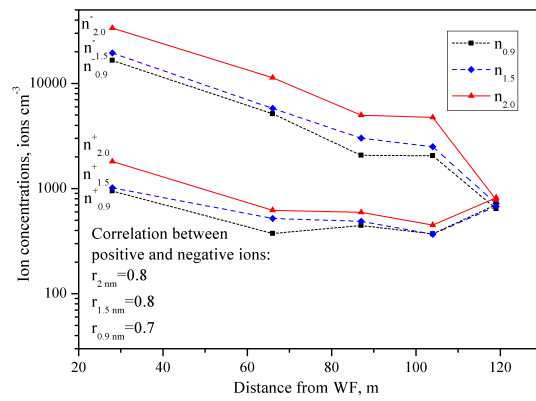


Fig. 11. Integral ion concentration gradients for ion diameter and polarity versus distance at the Gartl WF.

25323

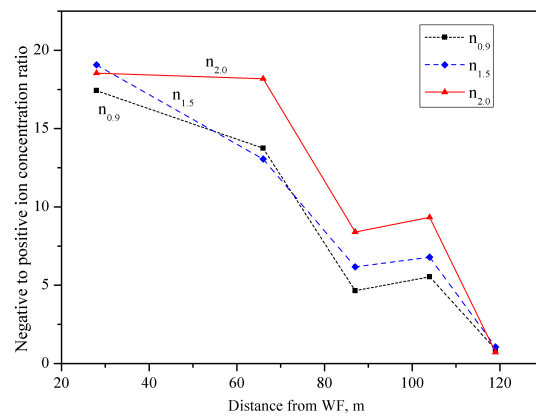


Fig. 12. Negative and positive ion concentration ratios versus distance at the Gartl WF.

25324

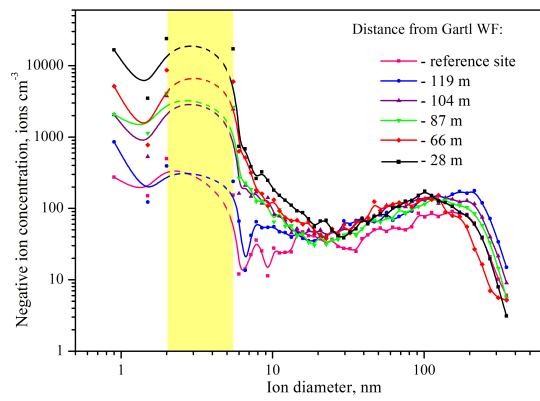


Fig. 13. Air ion concentrations vs. size for different distance measuring points at Gartl WF, Döllach. Shaded area indicates interpolated values (cubic B-spline) between CDI-06 (0.9–2.0 nm) and SMPS (5.5–350 nm) measurements. The reference site data series (magenta curve) represents the reference site where no WF generated ions were expected to occur.